JOURNAL OF Materials CHEMISTRY

Structure, texture, acidity and catalytic performance of $AlPO_4$–caesium oxide catalysts in 2-methyl-3-butyn-2-ol conversion

Felipa M. Bautista,[a] Juan M. Campelo,*[a] Angel Garcia,[a] Raquel M. Leon,[a] Diego Luna,[a] Jose M. Marinas,[a] Antonio A. Romero,[a] Jose A. Navio[b] and Manuel Macias[b]

[a]*Departamento de Química Orgánica, Facultad de Ciencias, Universidad de Córdoba, Avda. S. Alberto Magno, s/n°, E-14004 Córdoba, España*
[b]*Instituto de Ciencia de Materiales de Sevilla, Centro de Investigaciones Científicas 'Isla de la Cartuja', Avda. Américo Vespucio, s/n°, E-41092 Sevilla, España*

Received 28th September 1998, Accepted 22nd December 1998

A series of aluminium orthophosphate–caesium oxide systems with various caesium oxide loadings (5–30 wt%) were prepared by impregnation of $AlPO_4$ with a methanolic solution of caesium acetate and characterized by TG/DTA, XRD, DRIFT, Raman, SEM-EDX, XPS, ^{27}Al and ^{31}P MAS NMR and nitrogen adsorption. Aluminium orthophosphate remained amorphous with caesium oxide incorporation when calcined at 873 K for 3 h. After thermal treatment at 1423 K it crystallized in the tridymite form except for materials containing 30 wt% caesium oxide. DRIFT spectroscopy showed that the P–OH stretching vibration at 3670 cm^{-1} decreased in intensity with caesium oxide loading. Materials at 20–30 wt% caesium oxide did not exhibit any hydroxyl bands. Besides, Al and P atoms remained in tetrahedral coordination as in unmodified aluminium orthophosphate. Moreover, the incorporation of caesium oxide leads, simultaneously, to a progressive decrease in surface area and pore volume (larger at 30 wt% caesium oxide) as well as to an increase in the most frequently occurring pore radius. On the other hand, caesium oxide reduced both the number and strength of acid sites as the caesium content increased. Consequently, 2-methylbut-3-yn-2-ol (MBOH) underwent almost exclusively dehydration to 3-methyl-3-buten-1-yne (acid activity) on pure $AlPO_4$, whereas its modification with increasing amounts of caesium oxide developed $AlPO_4$-based materials with increased basic properties and hence high selectivities (99 mol%) to the base-catalysed cleavage of MBOH yielding acetone and acetylene.

Introduction

Amorphous aluminium orthophosphates can be used as catalysts and supports. As catalysts, they are active in several organocationic chemical processes in the gas phase and in the field of selective synthetic chemistry involving acid- and base-catalysed liquid-phase reactions.[1–3] Aluminium orthophosphates were also used as metal supports in the liquid-phase hydrogenation of the double bond of alkenes bearing a variety of organic functions.[4] Also, $AlPO_4$-supported zinc borohydride materials were active catalysts for the liquid-phase reductive cleavage of epoxides[5] and the hydration of aromatic alkenes and alkynes.[6] The modification of the acid–base properties of $AlPO_4$ by the incorporation of metal oxides (Al_2O_3, B_2O_3, TiO_2, ZrO_2, and ZnO), allowed us to control catalytic activity.[1–3]

Moreover, the development of solid base catalysts (alkaline earth metal oxides, rare earth metal oxides, modified zeolites and clays) has recently acquired great importance in the growing field of heterogeneous base catalysis for fine chemistry applications.[7–10] Thus, alkali metal ion-exchanged zeolites exhibited basic properties and promoted a number of base catalysed reactions but their basic sites were relatively weak. Caesium ions in excess of the ion-exchange capacity or caesium oxide impregnated zeolites generated stronger basic sites than those of simple alkali metal ion-exchanged zeolites, thus exhibiting high performance for reactions such as alcohol dehydrogenation,[11–13] side chain toluene alkylation,[14,15] Knoevenagel condensation of benzaldehyde with active methylene compounds,[16] 1-butene isomerization[17–19] and conversion of 2-methylbut-3-yn-2-ol into acetone and acetylene.[20] More recently, caesium oxide or caesium–lanthanum mixed oxides were introduced on SiO_2–Al_2O_3, γ-Al_2O_3 and MCM-41 molecular sieve[21–24] leading to catalysts with surface base properties showing interesting performances in Knoevenagel condensation of benzaldehyde with ethyl cyanoacetate,[21,24] Michael addition of ethyl cyanoacetate to ethyl acrylate[21,24] and rearrangement of ω-phenylalkanals into phenylmethyl ketones.[23]

In the present work a series of aluminium orthophosphate–caesium oxide systems with various caesium oxide loadings (5–30 wt%) were prepared by impregnation of $AlPO_4$ with a methanolic solution of caesium acetate and characterized by several physical methods. Also, we report on the effect of caesium oxide loading on the surface acid–base character by using pyridine chemisorption and the conversion of 2-methylbut-3-yn-2-ol (MBOH) as probe reaction. In this sense, Lauron-Pernot *et al.*[25–27] showed that MBOH is a very sensitive molecule for the simultaneous characterization of acidic and basic surface properties of solids. Thus, MBOH undergoes dehydration over solid acids yielding 3-methylbut-3-en-1-yne whereas over basic materials it gives acetone and acetylene. Moreover, the production of 3-hydroxy-3-methylbutan-2-one and/or 3-methylbut-3-en-2-one seems to be characteristic of amphoteric solids possessing acid–base ion pairs. A recent study[20] showed that this test was independent of the nature of the basic sites (Bronsted or Lewis) making it a global measure of basic properties. In our case, the MBOH conversion was studied in both pulse and flow reactors and, in flow experiments, a comparison with MgO, ZnO and γ-Al_2O_3 was also drawn.

Experimental

Catalysts

Two $AlPO_4$ supports with different pore properties were used. They were obtained by precipitation, from $AlCl_3{\cdot}6H_2O$ and H_3PO_4 (85 wt%) aqueous solutions, with ethylene (E) or propylene (P) oxide as described elsewhere.[1] The solid thus

obtained was washed with 2-propanol, dried at 393 K for 24 h and calcined at 923 K for 3 h.

$AlPO_4$–caesium oxide (5–30 wt% caesium oxide) catalysts were prepared by impregnation until incipient wetness using a methanolic solution of caesium acetate. The impregnated $AlPO_4$ were dried at 393 K (24 h) and then calcined at 873 K (3 h). Samples are denoted P (or E) followed by the caesium oxide loading (in wt%; 5Cs, 20Cs, and so on) and by the treatment temperature (P-5Cs-873, E-10Cs-873, *etc.*). Unmodified $AlPO_4$ (P-0 and E-0) were similarly prepared by placing them in methanol containing no caesium acetate.

Thermogravimetry and differential thermal analysis

Thermogravimetric (TG) and differential thermal analyses (DTA) were obtained simultaneously using a high-temperature Setaram 92, model 16.18 thermal analyzer, in the presence of static air at a heating rate of 10 K min^{-1} (temperature range: 273–1423 K). Finely powdered α-alumina was used as a reference material.

Gases evolved from TG experiments were analysed by mass spectrometry using a VG Sensorlab quadrupole mass spectrometer from Fisons Instruments plc/VG quadrupoles (East Sussex, UK) operating in the multiple-ion-monitoring (MIM) mode.

XRD Measurements

X-Ray powder diffractometry (XRD) was carried out at 300 K and in the 2θ range between 10 and 80° (at a scanning speed of 2° min^{-1}) using a Siemens D500 diffractometer equipped with Ni-filtered Cu-Kα radiation ($\lambda = 1.5405$ Å) at 35 kV and 20 mA. The crystalline XRD patterns were compared with JCPDS standards.

NMR Spectroscopy

^{27}Al (pulse; 0.6 μs; recycle delay; 0.3 s), ^{31}P (pulse; 2.6 μs; recycle delay: 6 s), ^{133}Cs (pulse; 3 μs; recycle delay; 3 s) and ^{1}H (pulse: 3 μs; recycle delay: 3 s) MAS NMR spectra were recorded at resonance frequencies v_0 of 104.26, 161.98, 52.48 and 400.13 MHz, respectively, with a Bruker ACP-400 multinuclear spectrometer (external magnetic field of 9.4 T). No mathematical procedures of NMR signal treatment were used. Also, the chemical shifts given for aluminium were not corrected for second-order quadrupole effects.

Measurements were carried out at room temperature with a standard Bruker double-bearing MAS (5.5 kHz) probe. About 200 mg of sample material were placed in the zirconium dioxide rotor (4 mm) with a volume of about 0.35 cm^3. The references for ^{27}Al, ^{31}P, ^{133}Cs and ^{1}H were $Al(H_2O)_6^{3+}$, 85% H_3PO_4, a 1 M aqueous solution of caesium chloride and TMS, respectively.

Scanning electron microscopy (SEM)

SEM studies were carried out in a JEOL apparatus, model JSM-5400, and the electron microprobe analysis (EPMA) was conducted by a Link Isis Pentafet Model analyzer. A semiautomatic image analyzer of magnetostrictive KONTRON MOP-30 board was used to estimate the average size of aggregates and particles.

XPS Measurements

The XPS spectra were recorded in a Leybold-Heraeus LHS-10 spectrometer working with a constant pass energy of 50 eV and using Al-Kα radiation ($h\upsilon = 1686.6$ eV) as the excitation source. Binding energy values were referred to the C(1s) peak (pollution carbon) at 284.6 eV.

DRIFT Measurements

DRIFT (diffuse reflectance infrared Fourier transform) spectra were recorded in a FTIR instrument (Bomen MB-100) equipped with an 'environmental chamber' (Spectra Tech, P/N 0030-101) placed in a diffuse reflectance attachment (Spectra Tech, Collector). A resolution of 8 cm^{-1} was used with 256 scans averaged to obtain a spectrum from 4000 to 400 cm^{-1}. Single-beam spectra were ratioed against KBr at the same temperature as that of the sample. A plot of pseudo-absorbance was preferred. This allowed direct subtraction of spectra obtained with the same sample under different conditions.

DRIFT spectra were recorded for all the calcined catalysts (200 mesh size and diluted to 15% in KBr) previously dried at 400 K for 24 h under vacuum. Afterwards, the catalyst was placed in the environmental chamber cell with a 20 mL min^{-1} flow of dehydrated and deoxygenated nitrogen, heated to 573 K and held at this temperature for 1 h prior to recording the spectrum. In some cases, spectra of the O–H stretching region were smoothed with a five-point Savitsky–Golay algorithm.[28]

Surface area and pore properties

Surface-area and pore-size information were obtained from N_2 adsorption–desorption isotherms at 77 K, using a Micromeritics ASAP 2000 analyzer. Prior to measurements, all samples were degassed to 0.1 Pa. Assessments of possible microporosity were made from *t*-plot constructions, using the Harkins–Jura correlation for t as a function of p/p_0. Parameters were fitted to a low-area, non-porous silica. Mesopore size distributions were calculated using the Barret–Joyner–Halenda (BJH) method,[29] the Halsey equation[30] and assuming a cylindrical pore model.

Surface acid properties

The surface acid properties of $AlPO_4$–caesium oxide catalysts were measured by using three procedures.

Pulse measurements. The surface acidity was measured in a dynamic mode by means of the gas-phase adsorption of pyridine (PY) at 373 K, using a pulse technique.[2] The pulse size was in the range of gas-chromatography linearity (pulse size *versus* detector response), corresponding to 0.1–0.5 monolayer. The acidity measurements were repeated several times and good reproducibility of the results was obtained (*ca.* 7%).

Temperature programmed desorption measurements. The TPD apparatus was described elsewhere.[31] After PY adsorption at 373 K, the weakly held PY was then eluted from the catalyst in a helium stream (50 mL min^{-1}) for 1 h. Afterwards the temperature was lowered to 323 K and thermal desorption experiments were carried out from 323 to 973 K at a rate of 10 K min^{-1} maintaining the temperature at 973 K for 10 min. Desorption was followed by a flame ionization detector. Repeated adsorption/TPD experiments using the same sample did not show any change in the desorption curve.

DRIFT measurements. DRIFT spectroscopy with adsorbed PY was carried out on pure catalysts previously dried at 400 K for 24 h under vacuum. Then, the catalyst was placed in the temperature/vacuum chamber cell and heated at 573 K (1 h) in dehydrated and deoxygenated nitrogen (20 mL min^{-1}). Afterwards, the reference DRIFT spectrum of the sample was recorded at the same temperature (573 K). Furthermore, the cell was sequentially cooled to 473 and to 373 K under nitrogen and the reference spectrum at each temperature was obtained.

The PY probe molecule (from a nitrogen flushed saturator) was adsorbed at 373 K for 2 h. This procedure gives the complete saturation of the catalyst surface as a large excess of

the probe molecule is admitted into the DRIFT cell. Physically adsorbed reagent was removed by flushing for 2–3 h with nitrogen. Longer nitrogen flushing times or vacuum treatment at 373 K did not modify the DRIFT spectra. The characteristic spectrum of the various forms of base retained on the catalyst was recorded. Subsequent flushings were performed at 473 and 573 K, and the corresponding spectra recorded at those temperatures taking the reference spectra at the same temperature.

Catalytic activity measurements

The catalytic properties of $AlPO_4$ and $AlPO_4$–caesium oxide catalysts in the conversion of 2-methylbut-3-yn-2-ol (MBOH) were studied by using a pulsed fixed bed reactor inserted between the sample inlet and the analytical column [15% TCPE/Supelcoport 80/200 (2 m × 1/8 in id)] of a HP-5890-II GC with flame ionization detection (FID). Catalytic measurements were performed under the following conditions: 2-methylbut-3-yn-2-ol (liquid) volume/pulse size; 1 μL; reaction temperature, 473–673 K (at 50 K intervals); catalyst weight, 10–30 mg in powder form; flow rate of nitrogen carrier gas, 30 mL min^{-1}. A fresh catalyst was used in each run, and before use the catalyst was pretreated by *in situ* heating under nitrogen (30 mL min^{-1}) for 1 h at 473 K.

Some reactions were also conducted in a continuous stainless-steel down-flow fixed-bed reactor (6 mm *id*) surrounded by an electric heater. An iron–constantan thermocouple was placed in the middle of the catalyst bed. The unit operated at atmospheric pressure. The substrate was delivered at a set flow rate (WHSV = 25.5 h^{-1}) using a liquid syringe pump (Harward Md. 44) and was vaporized prior to passing it through the catalyst bed in the presence of a flow of nitrogen carrier gas (3 L h^{-1}) regulated by mass-flow controllers. The catalyst charges (*W*) were small, usually 80 mg, retained by quartz wool at almost the center of the reactor. The reaction temperature was 573 K, except where otherwise specified. Standard catalyst pretreatment was carried out *in situ* at 573 K for 1 h under a stream of high purity nitrogen (99.999%, H_2O < 3 ppm).

Reaction products were analysed on-line by GLC with FID (Varian Md. 3400) and a column (2 m × 1/8 in id) packed with 15% TCPE/Supelcoport 80/200. Product characterization was performed by GC-MS (HP-5890 GC coupled with a HP-5970 MSD). Retention times were compared to those of commercially available reagents. Reaction products were 3-methylbut-3-en-1-yne, acetylene, acetone and minor amounts of 3-methylbut-3-en-2-one and 3-methylcrotonaldehyde. Blank runs showed that, under the experimental conditions used in this work, thermal effects could be ignored.

Results and discussion

TG and DTA measurements

The DTA profiles for P-0 and P-20Cs samples are shown in Fig. 1A whereas Fig. 1B shows the TG and DTG profiles for P-20Cs. Remaining P-Cs and E-Cs samples displayed almost the same behaviour.

TG profiles were characterized by two weight losses up to 773 K. The first one at 293–500 K (*ca.* 6% weight loss), accompanied by a DTG peak (≈440 K) and an endothermic DTA band (≈390 K), was attributed to the desorption of adsorbed water (Fig. 1C). The second weight loss (*ca.* 5%) at 500–773 K, also accompanied by a DTG peak (≈687 K) and an exothermic DTA band (≈710 K), is associated with combustion of acetate moieties into carbon dioxide and water as well as the desorption of acetic acid, as indicated in Fig. 1C, where it appeared to be continuous analysis, by mass spectrometry, of the gases evolved from P-20Cs sample during thermal treatment in the range 298–923 K (10 K min^{-1}). In this sense, mass spectrometry analysis of the gas phase revealed

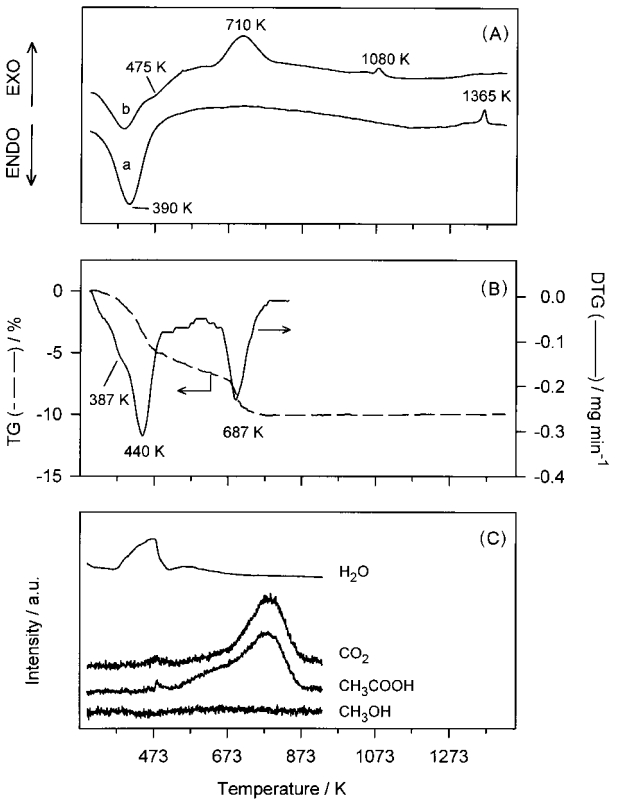

Fig. 1 (A) DTA curves (static air; 10 K min^{-1} scan): (a) P-0–873; (b) P-20Cs-873. (B) TG/DTG curves for P-20Cs-873 sample (static air; 10 K min^{-1} scan). (C) Mass spectrometry profiles (argon flow: 50 mL min^{-1}; 10 K min^{-1} scan).

that water (*m*/*z*: 18), carbon dioxide (*m*/*z*: 44) and acetic acid (*m*/*z*: 60) were by far the major desorption products. Methanol (*m*/*z*: 31) was not found. Therefore, these results allow us to verify our calcination procedure.

Moreover, between 773 and 1423 K, a slight weight loss (<0.02%) was observed, due mainly to the condensation of surface hydroxyls, together with an exothermic DTA band. The exothermic transition corresponded to the crystallization of the amorphous $AlPO_4$ into tridymite-$AlPO_4$ and/or α-crystobalite-$AlPO_4$ crystalline forms (see XRD results below). The position of this exothermic band also depended on the caesium loading and thus, as the caesium oxide loading increased up to 20 wt%, the exothermic peak decreased in intensity and shifted to lower temperatures: 1365, 1195, 1145 and 1080 K for P-0, P-5Cs, P-10Cs and P-20Cs, respectively. P-30Cs and E-30Cs samples did not exhibit any exothermic bands at temperatures above 873 K and remained in a low degree of crystallinity even at 1423 K (see XRD results).

XRD Measurements

XRD patterns of all $AlPO_4$–caesium oxide systems calcined at 873 K for 3 h (results not shown) exhibited only a very broad band in the range 2θ from 15 to 30°, a characteristic of the amorphous $AlPO_4$. Besides, the peaks of caesium oxide (ASTM, 9–104) were absent indicating that caesium oxide also exhibited a low degree of crystallinity and high dispersion.

Moreover, from Fig. 2 it can be seen that the thermal treatment at temperatures above those of the DTA peaks (1423 K) developed bands corresponding to crystalline $AlPO_4$. The structure of P-Cs (Fig. 2) samples corresponded to that of the pseudohexagonal tridymite identified by its characteristic reflections at *d* = 4.34 (2θ = 20.4), 4.11 (2θ = 21.6) and 3.83 Å (2θ = 23.2°) [ASTM, 20–45] although the relative intensities differed from those reported by Florke.[32] In E-Cs samples

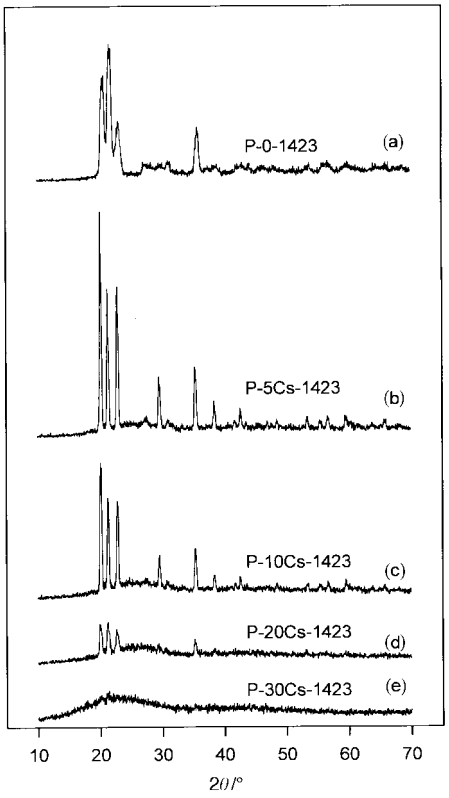

Fig. 2 XRD profiles of P-Cs materials after DTA measurements (Cu-Kα, $\lambda = 1.5405$ Å): (a) P-0–1423; (b) P-5Cs-1423; (c) P-10Cs-1423; (d) P-20Cs-1423; (e) P-30Cs-1423.

(results not shown) $AlPO_4$ crystallized in a mixture of tridymite and α-crystobalite forms. The α-crystobalite form[33] was identified by its characteristic reflections at $d = 4.07$ ($2\theta = 21.9$) and 2.51 Å ($2\theta = 35.8°$) [ASTM, 11–500].

Furthermore, the XRD diagrams of P-30Cs (Fig. 3) and E-30Cs (not shown) samples thermally treated in the range 1018–1423 K, which did not exhibit any DTA exothermic peaks above 800 K, indicated partial $AlPO_4$ crystallization so that these systems remained at a low degree of crystallinity.

^{27}Al, ^{31}P and ^{133}Cs MAS NMR Spectroscopy

The ^{27}Al MAS NMR spectra (not shown) of $AlPO_4$ and $AlPO_4$–caesium oxide samples calcined at 873 K for 3 h exhibited a broad peak at around δ 39, typical of tetrahedral aluminium with phosphorus in the second coordination sphere, *i.e.* sharing oxygens with four tetrahedra of phosphorus [$Al(OP)_4$].[34,35] Moreover, the ^{31}P MAS spectra (not shown) also exhibited one single component at around δ −27. This chemical shift corresponded to P atoms in tetrahedral co-ordination with P–O–Al bonds [*i.e.* $P(OAl)_4$ environments]. Therefore, the incorporation of caesium did not change the isotropic chemical shift value of the ^{27}Al and ^{31}P peaks so that the local structure of the $AlPO_4$ support was not changed by caesium.

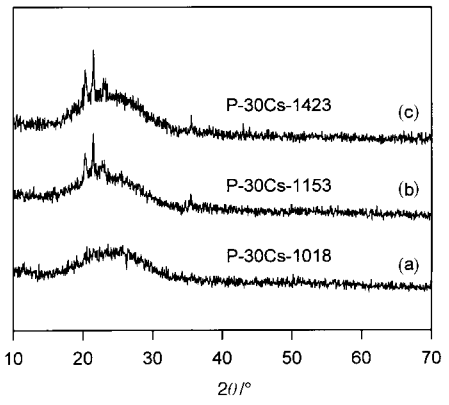

Fig. 3 XRD profiles (Cu-Kα, $\lambda = 1.5405$ Å) of P-20Cs sample thermally treated at increasing temperatures: (a) P-30Cs-1018; (b) P-30Cs-1153; (c) P-30Cs-1423.

On the other hand, the ^{133}Cs MAS NMR spectra (not shown) exhibited a non-resolved very broad gaussian band centered at around δ −30 (full width half maximum: 176 ppm) for E-30Cs-873 and P-30Cs-873 samples. Thus, the caesium was in chemical environments of low symmetry (highly dispersed caesium oxide species bonded in different ways to the $AlPO_4$ support). As the amount of caesium oxide increased in $AlPO_4$ the ^{133}Cs resonance shifted to a lower field. This change in peak position had been attributed to the interaction of caesium with neighboring caesium atoms.[24]

Furthermore, the ^{1}H spectra (not shown) of E-0–873 and P-0–873 samples [amorphous $AlPO_4$; surface composition (XPS) P/Al ≈ 0.90] contained a small line from Al–OH groups (at around δ −0.9) and an unresolved peak from P-OH groups (at around δ 3.6), as described by Mastikhin *et al.*[36] Besides, the peak at $\delta \approx 3.6$ decreased sharply in intensity with caesium loading. At 20–30 wt% caesium oxide both ^{1}H signals disappeared indicating that chemical interaction of the supported caesium oxide species takes place with Al-OH and P-OH groups. These results were confirmed by DRIFT spectroscopy (see below).

SEM, EPMA and XPS Studies

SEM micrographs of E-30Cs-873 and P-30Cs-873 samples are shown in Fig. 4. SEM observation showed a very widely varied distribution in morphology, texture and particle sizes for all $AlPO_4$–caesium oxide samples. Besides, no changes were observed either in morphology or in particle sizes when the amount of caesium increased. The average size of the biggest particles was around 40 μm, although a large population of small particles was observed in all samples.

Table 1 summarizes the information about the elemental surface composition (EPMA) and XPS binding energies (in parentheses) of the elements present on the surface of E-Cs-873 and P-Cs-873 samples. Thus, Table 1 indicates a surface enrichment in caesium compared to bulk values. However, there was a homogeneous distribution of caesium so that the surface composition of different particles remained almost unchanged.

On the other hand, as can be seen from Table 1, the surface concentration ratio $[P]_s/[Al]_s$ of E-Cs-873 and P-Cs-873 samples decreased with caesium loading. This could be accounted for by the fact that caesium interacted preferentially with surface P–OH groups (see ^{1}H NMR and DRIFT results). Furthermore, the various core lines investigated for different samples were very similar and they all appeared as single XPS symmetrical lines, indicating homogeneous distribution of the electron densities around the atoms throughout the solid.

DRIFT Measurements

The DRIFT spectrum of pure amorphous $AlPO_4$ (P-0–873 sample), recorded after pretreatment at 573 K (1 h) under a nitrogen stream (20 mL min^{-1}), is shown in Fig. 5(a) [the DRIFT spectra of E-0–873 samples was similar]. In the OH stretching region (4000–2500 cm^{-1}) two isolated hydroxyl peaks were found: a weak one at 3793 cm^{-1} and a strong one at 3670 cm^{-1}, which were due to surface Al–OH (with aluminium atoms in tetrahedral co-ordination) and of non-bonded surface P–OH groups, respectively.[37] There is also a broad band around 3538 cm^{-1} due to bonded hydroxyl groups.

The DRIFT spectra of the hydroxyl region of P-Cs-873 samples are shown in Fig. 5(b)–(e). The incorporation of

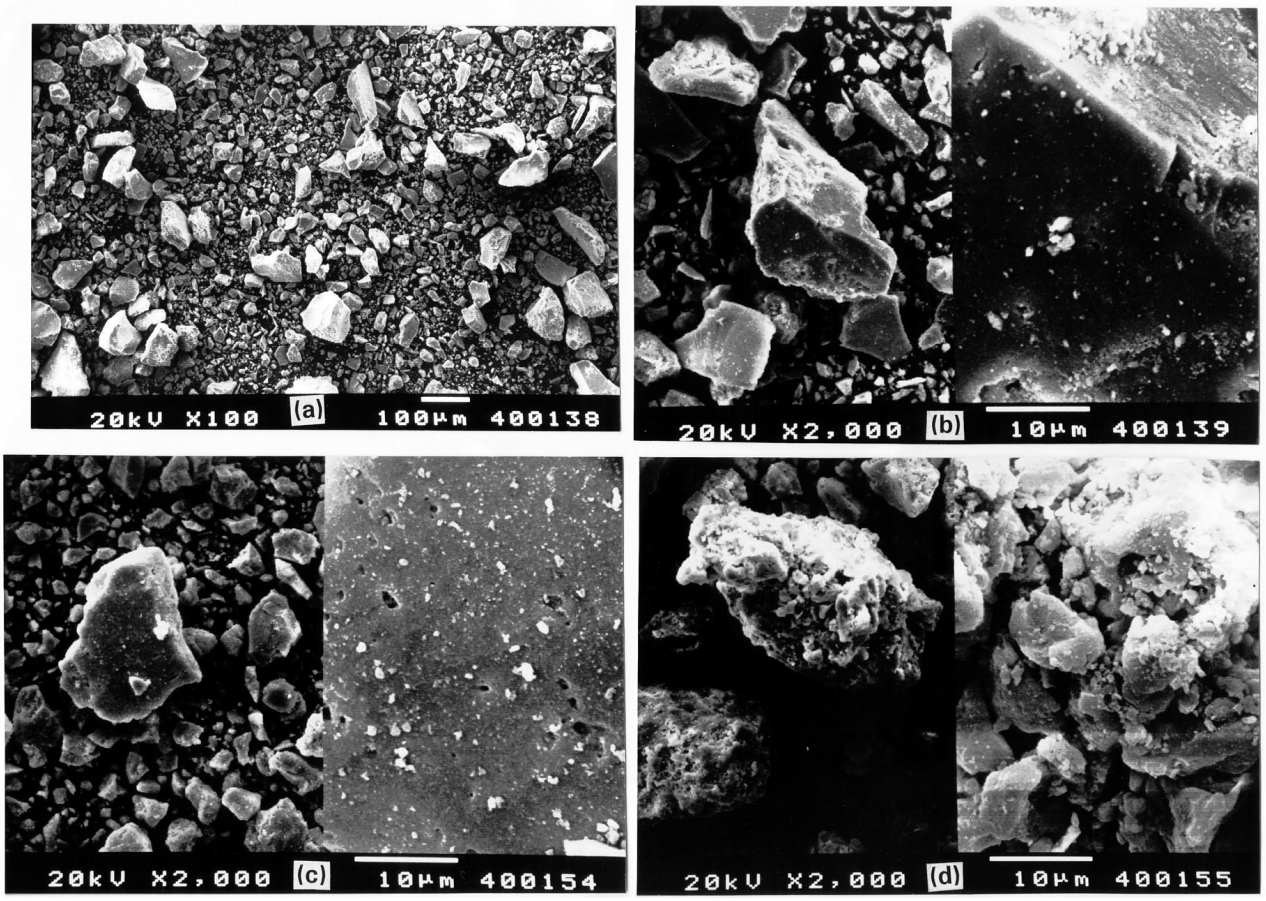

Fig. 4 SEM micrographs: (a), (b) E-30Cs-873; (c), (d) P-30Cs-873.

Table 1 Electron microprobe analysis and XPS binding energies[a] of the elements present on the surface of E-Cs-873 and P-Cs-873 systems

System	P (2p) (at%)	Al (2p) (at%)	Cs[b] (at%)	Cs (3d) (at%)	$[P]_s/[Al]_s$
E-0–873	15.9 (133.6)	17.7 (74.1)	—	—	0.90
E-5Cs-873	14.9 (133.2)	18.5 (74.1)	0.7 (723.8)	1.0	0.81
E-10Cs-873	14.5 (133.0)	18.0 (74.1)	1.5 (723.8)	2.7	0.81
E-20Cs-873	14.0 (133.0)	18.4 (74.1)	3.2 (723.8)	3.0	0.76
E-30Cs-873	12.9 (132.9)	17.6 (74.1)	5.3 (723.7)	7.2	0.73
P-0–873	15.8 (133.6)	17.9 (74.1)	—	—	0.88
P-5Cs-873	14.8 (133.2)	18.4 (74.1)	0.7 (723.7)	1.4	0.80
P-10Cs-873	14.7 (133.1)	18.3 (74.1)	1.5 (723.7)	1.8	0.80
P-20Cs-873	13.1 (133.0)	18.4 (74.1)	3.2 (723.7)	5.5	0.71
P-30Cs-873	12.8 (132.8)	18.4 (74.1)	5.3 (723.6)	7.9	0.70

[a] In parentheses, eV. [b] Bulk values.

increased amounts of caesium oxide results in the disappearance of Al-OH and P-OH bands, so that P-20Cs-873 and P-30Cs-873 samples did not exhibit any hydroxyl bands (E-Cs samples exhibited the same trend). This is consistent with ^{1}H NMR results.

Moreover, the DRIFT spectra of the skeletal region (below 2500 cm^{-1}) showed that, in all E-Cs and P-Cs [Fig. 5(b)–(e)] samples, the phosphorus atom was surrounded by tetrahedra of oxygen atoms: bands due to the triply degenerate P–O stretching vibration (1069 cm^{-1}), v_3 mode of tetrahedral PO_4^{3-}; triply degenerate O–P–O bending vibration (478 cm^{-1}), v_4 mode of PO_4^{3-} tetrahedra and stretching vibration of Al–O bonds in combination with P-O bonds (691 cm^{-1}). DRIFT data were in accordance with the XRD and ^{27}Al and ^{31}P MAS NMR data.

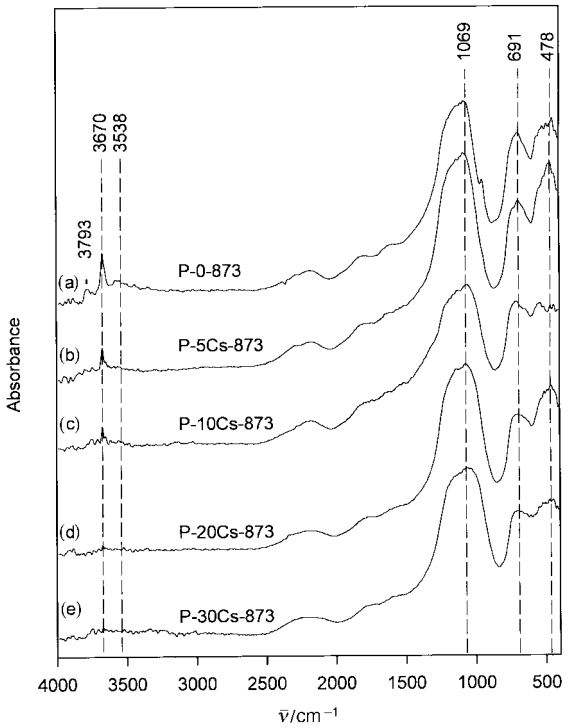

Fig. 5 DRIFT spectra (at 573 K; nitrogen flow 20 mL min^{-1}): (a) P-0–873; (b) P-5Cs-873; (c) P-10Cs-873; (d) P-20Cs-873; (e) P-30Cs-873. All spectra were displaced for presentation.

Surface area and pore properties

The adsorption–desorption isotherms of $AlPO_4$ and $AlPO_4$–caesium oxide samples calcined at 873 K for 3 h were of nearly the same type with closed and well defined hysteresis loops (Fig. 6A). From the shape of the curves it can be assumed that samples consist mainly of mesopores, showing type IV isotherms in the BDDT classification[38] and hysteresis loops of *H1* type according to the IUPAC classification.[39] Moreover, the pore volume (at $p/p_0=0.99$) decreased while the starting point of the hysteresis loop was displaced towards higher relative pressures on increasing caesium loading (Fig. 6A shows the evolution of the shape of the P-Cs sample isotherm on increasing caesium content). These facts could be accounted for by a continuous restructuring of the porous texture as well as an increase in mesopore diameter (Fig. 6B) in accord with XRD and ^{133}Cs MAS NMR results.

The *t* plots (not shown), using the Harkins–Jura correlation[40] for *t* as a function of p/p_0 show two steps, the highest (an upward deviation from the linear branch of the *t* plot with ascending *t* values) corresponding to capillary condensation (which starts at relative pressures similar to those of the corresponding hysteresis loops) and the lowest (linear *t* plot passing through the origin) corresponding to a mono-multilayer adsorption mechanism on pores in which the adsorption desorption was reversible, thus confirming the mesoporous texture of the solids and the absence of microporosity. Furthermore, the surface areas calculated by the *t* method from the slopes of the straight lines were found to tally with those obtained by the BET (Brunauer–Emmett–Teller) method. This reflects that the samples were free from micropores as well as the high accuracy of the C_{BET} determination.

The porous texture of the E-Cs-873 and P-Cs-873 samples was analysed following the BJH method and assuming a cylindrical pore model.[29] The analysis was applied to the adsorption branch of each isotherm, which is to be preferred to the desorption branch for type IV isotherms.[41,42]

The BET surface area (S_{BET}), pore volume (V_P, at $p/p_0=$ 0.99), C_{BET} constant and mesopore diameter (D) are collected in Table 2. Here it can be seen that the incorporation of caesium oxide into $AlPO_4$ leads, simultaneously, to a progressive decrease in surface area and pore volume. This decrease was larger in E-Cs samples. Moreover, the decrease in surface area was more pronounced as the caesium oxide loading of catalyst was increased (for example, in P-Cs samples, the incorporation of caesium oxide at 5, 10, 20 and 30 wt% resulted in a loss of surface area of 12, 27, 49 and 77%, respectively) due to the surface restructuring although the amorphous character and Al and P tetrahedral environments remained unchanged. Fig. 6B shows that the pore size distribution as well as the full width half maximum were displaced towards higher values as the caesium amount increased. Also, the C_{BET} value increased with caesium loading, which means that the presence of caesium enhanced the adsorbate–adsorbent interaction.

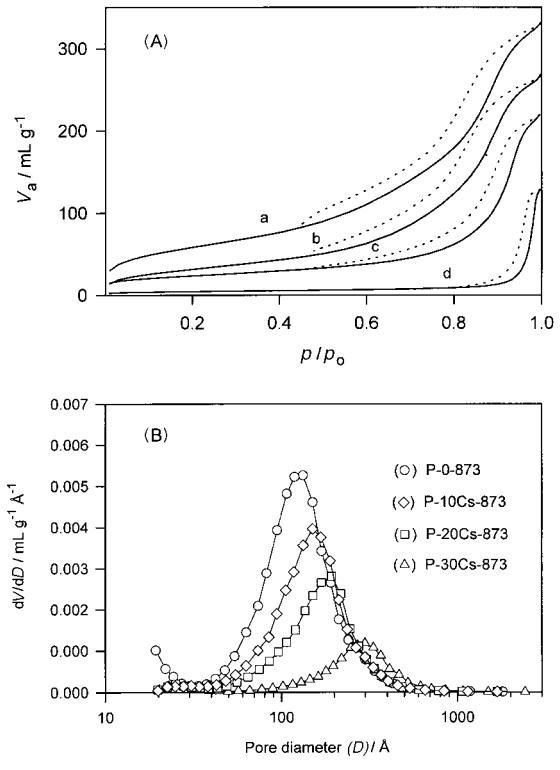

Fig. 6 (A) Adsorption–desorption isotherms and (B) pore size distributions: (a, ○) P-0-873; (b, ◇) P-10Cs-873; (c, □) P-20Cs-873; (d, △) P-30Cs-873.

Table 2 Textural properties, surface acidity *vs.* pyridine and rate constants (k_a) in MBOH conversion of $AlPO_4$ and $AlPO_4$–caesium oxide catalysts

Catalyst	S_{BET}/ m^2 g^{-1}	V_P/ mL g^{-1}	D/ nm	C_{BET}	PY[a] μmol g^{-1}	10^6[b]/k_a mol s m^2 atm^{-1}
P-0–873	209	0.79	13.5	81	377	4.5
P-5Cs-873	185	0.73	15.4	142	215	2.0
P-10Cs-873	153	0.65	15.1	197	151	0.7
P-20Cs-873	107	0.53	18.9	240	39	0.3
P-30Cs-873	48	0.36	30.4	239	4	0.4
E-0–873	218	0.53	4.8	80	421	4.5
E-5Cs-873	185	0.46	5.4	95	346	3.0
E-10Cs-873	151	0.43	6.8	128	163	1.0
E-20Cs-873	84	0.34	17.9	212	34	0.2
E-30Cs-873	16	0.20	—[c]	279	—[d]	0.1

[a]Adsorption temperature: 373 K. [b]At a reaction temperature of 573 K. [c]Macroporous. [d]There was no adsorption of titrant.

Surface acidity measurements

The surface acidity (Brønsted and Lewis acid sites) of E-Cs-873 and P-Cs-873 samples is given in column six of Table 2 as the amount of pyridine (PY) chemisorbed at saturation at 373 K.[2] It is evident that the incorporation of caesium oxide into $AlPO_4$ resulted in a remarkable decrease in surface acidity, that was more pronounced as the caesium oxide loading of catalyst increased.

The thermodesorption of PY from E-Cs-873 and P-Cs-873 samples resulted in a number of overlapping peaks, generating complex thermodesorption spectra. Fig. 7 presents characteristic PY thermal desorption profiles (P-Cs-873 samples) obtained after adsorption of PY at 373 K employing a heating rate of 10 K min^{-1}. In order to make the comparisons easier,

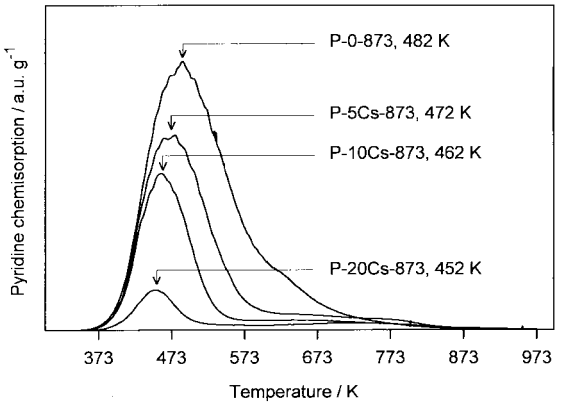

Fig. 7 PY TPD profiles for P-0–873, P-5Cs-873, P-10Cs-873 and P-20Cs-873.

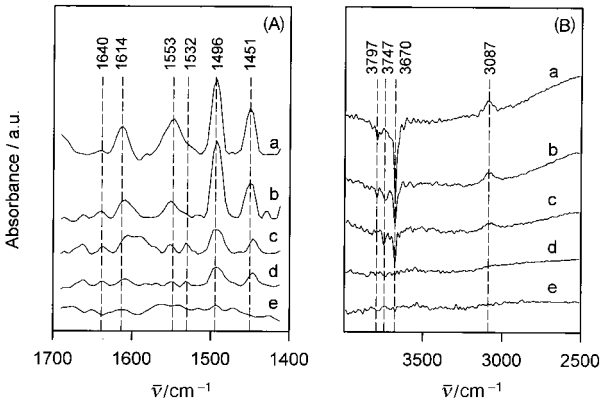

Fig. 8 DRIFT spectra of adsorbed PY (at 573 K; nitrogen flow 20 mL min^{-1}). (A) Skeletal region and (B) OH stretching region: (a) P-0–873; (b) P-5Cs-873; (c) P-10Cs-873; (d) P-20Cs-873; (e) P-30Cs-873.

areas under the experimental desorption spectra were normalized to catalyst weight.

TPD measurements indicated that, as the caesium oxide content was raised from 5 to 20 wt%, the total amount of PY was remarkably reduced and the peak maximum temperature of PY desorption shifted to lower temperatures, corroborating acidity measurements.

The adsorption of PY was also studied by DRIFT spectroscopy using a temperature controlled cell under a nitrogen atmosphere. Fig. 8A shows the spectra (1700–1400 cm^{-1}) of the P-0–873 and P-Cs-873 samples after adsorption and desorption of PY at 373 K. On sample P-0–873 [Fig. 8A(a)], PY adsorption at 373 K, followed by desorption at the same temperature for 1 h, gives rise to the characteristic upward absorption bands of PY interacting with Brønsted acid sites at 1553 and 1640 cm^{-1} (due to the ν_{19b} and ν_{8a} modes of the pyridinium ions) and of species coordinated to Lewis acid sites at 1451 and 1614 cm^{-1} (due to the ν_{19b} and ν_{8a} modes of coordinated pyridine).[43,44] A band at 1490 cm^{-1}, which can be attributed to PY chemisorption on Brønsted and/or Lewis acid sites, was also found. Simultaneously with the appearance of these bands, the OH stretching vibration bands of the P–OH (3670 cm^{-1}) and Al–OH groups (3797 and 3747 cm^{-1}, due to tetrahedral and octahedral coordination, respectively) disappeared. As the reference spectrum was acquired from the fresh catalyst, in the DRIFT spectrum after PY adsorption the Al–OH and P–OH bands appeared as downward bands [Fig. 8B(a)]. This means that PY indeed interacted with hydroxyl groups on the P-0–873 and E-0–873 samples. In addition, a weak band at 3087 cm^{-1} was due to C–H stretching vibration of the pyridine aromatic ring.

Moreover, Fig. 8A(b)–(e) shows that the incorporation of increased amounts of caesium oxide resulted in a strong decrease in the absorption intensity of both Brønsted-bound (1553 cm^{-1}) and Lewis-bound (1451 cm^{-1}) PY. Besides, the amount of Brønsted-bound PY decreased faster than Lewis-bound PY, indicating that the Lewis acid sites were stronger than the Brønsted ones. However, for the P-30Cs-873 sample, PY absorption bands completely disappeared. Furthermore, for all P-Cs-873 and E-Cs-873 samples, adsorbed PY was easily removed by treatment at 473 K for 1 h under nitrogen. So, the changes in band intensities with caesium oxide loading can be associated fairly well with the changes in acid characteristics detailed in column six of Table 2 and in Fig. 7 (TPD measurements).

Catalytic measurements

The use of model reactions was recommended[45] as the best method for characterizing industrial catalysts. Thus, reactions

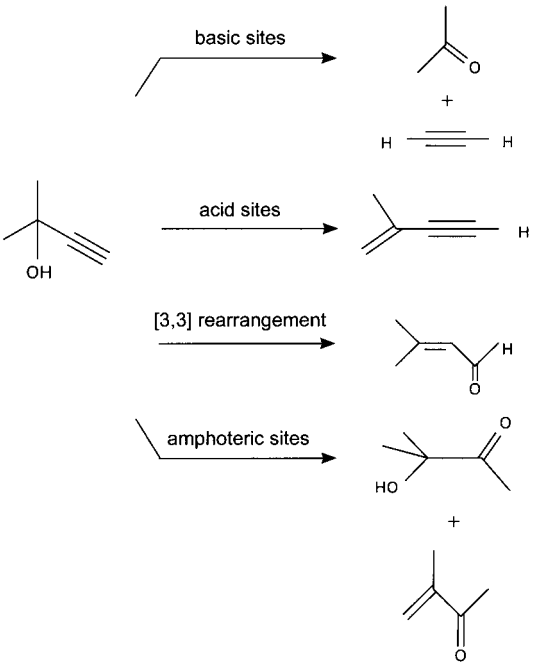

Fig. 9 Overall reaction scheme for 2-methylbut-3-yn-2-ol (MBOH) conversion.

such as skeletal isomerization of 3,3-dimethylbut-1-ene and cyclohexene, cracking/isomerization of 2-methylpentane and *n*-hexane or isomerization/disproportionation of *o*-xylene were used to characterize the acidity and acid strength of protonic sites. Later on, Lauron-Pernot *et al.*[25–27] showed that the conversion of 2-methylbut-3-yn-2-ol (MBOH) can be used as a probe reaction for the simultaneous characterization of acidic and basic surface properties of solid catalysts. This molecule undergoes dehydration over solid acids yielding 3-methylbut-3-en-1-yne whereas over basic materials it gives acetone and acetylene. In this latter case there was no difference in product selectivity between Lewis (MgO) and Brønsted [KOH/SiO_2 and $Ca(OH)_2$] bases.[20] Moreover, the formation of 3-hydroxy-3-methylbutan-2-one and/or 3-methylbut-3-en-2-one seems to be characteristic of amphoteric solids possessing acid–base ion pairs.[27] Furthermore, 3-methylcrotonaldehyde (prenal) can also be obtained by acid [3,3]-rearrangement.[46] The overall reaction scheme appeared in Fig. 9.

Here we report on the results of MBOH conversion, selected as a dynamic method, for further characterization of the surface acid–base properties of $AlPO_4$ catalysts modified by caesium oxide loading.

In the absence of boundary, inter- and intra-particle diffusion effects, the MBOH conversion reaction data (pulse measurements) for all $AlPO_4$–caesium oxide catalysts were found to fulfil the Bassett–Habgood rate equation[47] for first-order reactions where the partial reaction pressure is low and the adsorption rate is faster than the rate of surface reaction, the latter being the rate-determining step. In this sense, only the data for 3–20 mol% total conversion were used for the calculation. The Bassett–Habgood equation was in the form

$$\ln [1/(1-X_T)] = k_a RT(W/F)$$

where X_T is total conversion, k_a the apparent rate constant of both acid and base surface processes, W the catalyst weight, and F the flow rate of carrier gas.

The apparent rate constants, k_a, were obtained from the slopes of the linear plots of $\ln [1/(1-X)]$ *vs.* W for X_T less than 20 mol%, where the equilibrium reaction can be neglected. The values obtained at 573 K for the different $AlPO_4$–caesium oxide catalysts are collected in the last column of Table 2. It

Table 3 Reaction selectivities (in pulse reactor; at different MBOH conversions) of $AlPO_4$ and $AlPO_4$–caesium oxide catalysts

	3 mol%				10 mol%				15 mol%				25 mol%			
Catalyst	S_{ACID}	S_{BASE}	S_{AMPH}	S_{CROT}	S_{ACID}	S_{BASE}	S_{AMPH}	S_{CROT}	S_{ACID}	S_{BASE}	S_{AMPH}	S_{CROT}	S_{ACID}	S_{BASE}	S_{AMPH}	S_{CROT}
P-0–873	98.0	1.5	0.4	0.1	98.1	1.4	0.3	0.2	97.8	1.4	0.3	0.4	98.0	1.2	0.3	0.5
P-5Cs-873	94.0	5.4	0.5	0.1	96.0	3.2	0.6	0.2	97.0	2.4	0.6	—	96.8	2.0	0.6	0.6
P-10Cs-873	86.0	10.4	1.9	1.7	86.7	9.3	2.1	1.9	87.4	8.7	2.0	1.8	88.7	7.4	2.1	1.8
P-20Cs-873	38.1	60.0	1.4	0.5	37.1	60.6	1.4	0.9	33.9	64.2	1.2	0.7	32.4	65.9	1.1	0.7
P-30Cs-873	0.2	99.8	—	—	0.4	99.6	—	—	0.8	99.2	—	—	0.7	99.3	—	—
E-0–873	98.7	0.8	0.3	0.2	98.5	0.9	0.4	0.2	98.3	0.9	0.5	0.3	98.3	1.0	0.5	0.3
E-5Cs-873	97.7	1.5	0.5	0.3	97.8	1.2	0.6	0.4	97.7	1.0	0.5	0.8	97.4	1.0	0.6	1.0
E-10Cs-873	92.4	4.7	1.0	1.9	92.2	4.8	1.0	2.0	92.2	4.4	1.2	2.2	92.2	4.5	1.4	1.9
E-20Cs-873	74.6	23.4	2.0	—	70.7	27.2	2.0	—	66.2	31.8	2.0	—	60.3	38.1	1.5	—
E-30Cs-873	1.2	98.8	—	—	1.2	98.8	—	—	1.0	99.0	—	—	0.9	99.1	—	—

was found that the rate constants decreased as caesium oxide loading increased. Besides, as was to be expected there was a fairly good relation between the catalytic activity of investigated samples (except for samples with 30 wt% caesium oxide loading) and the amount of PY chemisorbed at 573 K (Table 2), where dehydration to 3-methylbut-3-en-1-yne was predominant. Nevertheless, P-20Cs-873 and P-30Cs-873 samples showed more activity (base-catalysed) than E-20Cs-873 and E-30Cs-873 ones. This fact could be explained due to better textural properties in P-Cs samples, thus favoring a better dispersion of the caesium oxide.

As far as selectivity of MBOH conversion was concerned, Table 3 compares product selectivities (S_{ACID}, S_{BASE}, S_{AMPH} and S_{CROT}) at four similar conversion levels (3–25 mol%) from pulse measurements.

As can be seen on pure $AlPO_4$, MBOH underwent dehydration to 3-methylbut-3-en-1-yne (S_{ACID}) exclusively. The incorporation of increasing amounts of caesium oxide into $AlPO_4$ produced a continuous decrease in the dehydration selectivity whereas the selectivity for the base-catalysed cleavage to acetone and acetylene (S_{BASE}) increased. In all cases, the selectivities to 3-methylbut-3-en-2-one (S_{AMPH}) and 3-methylcrotonaldehyde (S_{CROT}) remained very low. Besides, selectivities did not show significant changes within the 3–25 mol% conversion range.

Table 4 Rate constants (k_a, at 573 K) and reaction selectivities (S) in MBOH conversion (flow measurements, WHSV = 25.5 h^{-1}) over P-0–873, P-30Cs-873, MgO, ZnO and γ-Al_2O_3 catalysts

		Reaction selectivities (mol%)			
Catalyst	10^6[a]/k_a/mol g^{-1} s^{-1}	S_{ACID}	S_{BASE}	S_{AMPH}	S_{CROT}
P-0–873	31.4	91.2	1.0	1.2	6.6
P-30Cs-873	7.3	0.5	99.4	—	0.1
P-30Cs-873[b]	108.4	0.3	99.6	—	0.1
MgO	114.6	—	100.0	—	—
ZnO	30.5	2.6	96.8	0.5	0.1
γ-Al_2O_3	8.3	12.1	82.0	4.4	1.5

[a]Time on-stream: 2 h. [b]At a reaction temperature of 623 K.

Moreover, MBOH conversions in a flow-reactor (WHSV = 25.5 h^{-1}; 573 K), fitted by a first-order rate equation, corroborated pulse data. The activity profiles, as a function of time on stream, for MBOH conversion on MgO, ZnO, γ-Al_2O_3 and

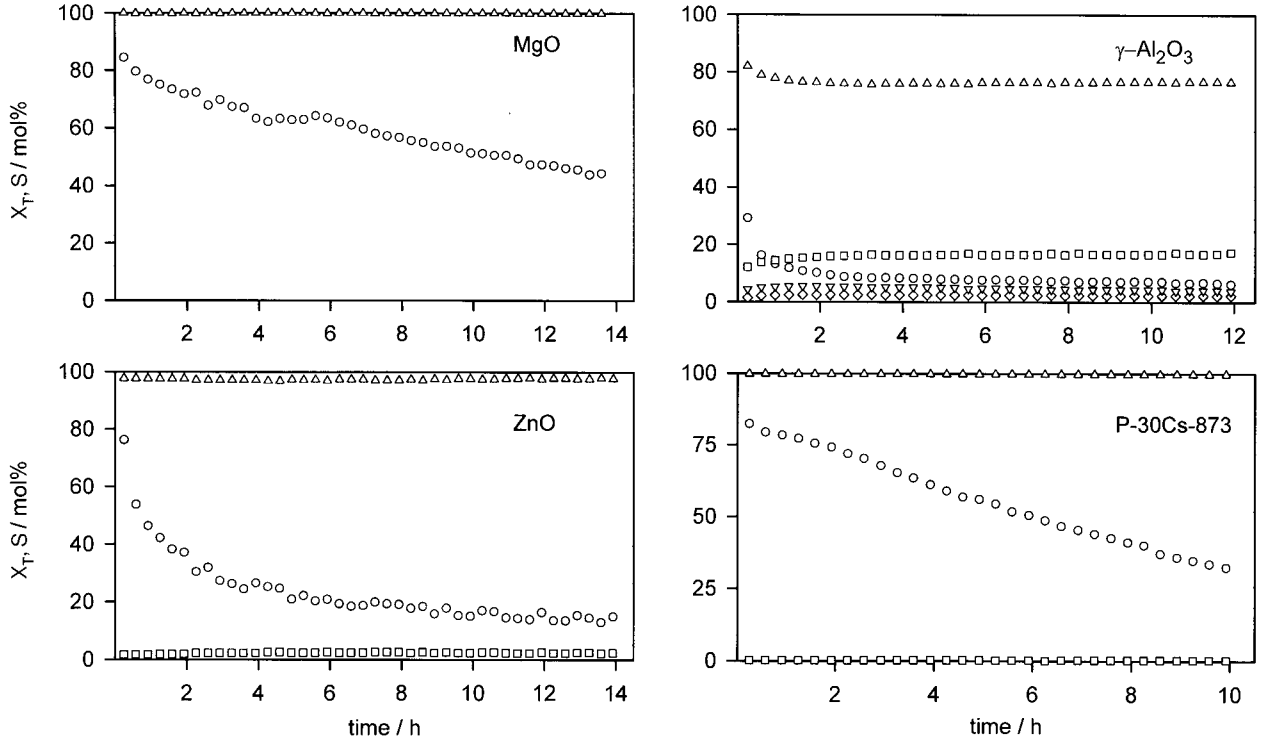

Fig. 10 Reaction profiles in 2-methylbut-3-yn-2-ol (MBOH) conversion on MgO, ZnO, γ-Al_2O_3 and P-30Cs-873 catalysts: (○) total conversion, X_T; (□) selectivity to 3-methylbut-3-en-1-yne, S_{ACID}; (△) selectivity to acetone and acetylene, S_{BASE}; (▽) selectivity to 3-methylbut-3-en-2-one; (◇) selectivity to 3-methylcrotonaldehyde (prenal).

P-30Cs-873 presented in Fig. 10 whereas the reaction rate constants, after 2 h on stream, are listed in Table 4. Table 4 compared also the product selectivities (S_{ACID}, S_{BASE}, S_{AMPH} and S_{CROT}), at 25 mol% MBOH conversion level, for P-0–873, P-30Cs-873, MgO, ZnO and γ-Al_2O_3 catalysts.

As can be seen from Fig. 10, the MBOH conversion decreased with the time on-stream although the selectivities for dehydration to 3-methylbut-3-en-1-yne (S_{ACID}) and for the base-catalysed cleavage (retrocondensation) to acetone and acetylene (S_{BASE}) did not show any change within 2–13 h on stream. Moreover, MBOH conversion increased strongly with temperature although the activity decay with time on-stream was also very important.

Furthermore, as can be seen from Table 4, P-30Cs-873 catalyst showed rate constants and reaction selectivities similar to those of typical solid base catalysts, such as MgO, when the reaction temperature was increased to 623 K. However, in all cases, the activity decay was important.

Conclusion

The $AlPO_4$–caesium oxide (5–30 wt% caesium oxide) materials remained amorphous when calcined at 873 K. Also, there was a surface enrichment in caesium compared to bulk values, although there was a homogeneous distribution of caesium when compared to that of different particles. Moreover, caesium interacted preferentially with P–OH groups. The incorporation of caesium oxide leads, simultaneously, to a progressive decrease in surface area and pore volume (larger at 30 wt% caesium oxide) as well as to an increase in the most frequently occurring pore radius. Besides, caesium oxide reduced both the number and strength of acid sites for as long as the caesium content increased. Thus, 2-methylbut-3-yn-2-ol underwent dehydration to 3-methylbut-3-en-1-yne (acid activity) almost exclusively on pure $AlPO_4$ whereas its modification with increasing amounts of caesium oxide developed $AlPO_4$-based materials with increased basic properties and hence high selectivities to the base-catalysed cleavage of MBOH yielding acetone and acetylene (99 mol% for E-30Cs-873 and P-30Cs-873 catalysts). So, the incorporation of caesium oxide provided a means of controlling the surface acid–base characteristics of $AlPO_4$ in order to achieve typical solid acid or solid base catalysts.

Acknowledgements

The authors acknowledge subsidies from the DGESIC (Project PB97/0446), Ministerio de Educacion y Cultura, and from the Consejeria de Educación y Ciencia (Junta de Andalucia), España. The authors also thank Dr. R. Ruiz (NMR Service, Universidad de Córdoba) for performing MAS NMR measurements. They also would like to thank Professor M. Sullivan for linguistic revision of the manuscript.

References

1 A. Blanco, J. M. Campelo, A. Garcia, D. Luna, J. M. Marinas and A. A. Romero, *J. Catal.*, 1992, **137**, 51 and ref. therein.
2 F. M. Bautista, J. M. Campelo, A. Garcia, D. Luna, J. M. Marinas, A. A. Romero, J.A. Navio and M. Macias, *J. Catal.*, 1998, **173**, 333 and ref. therein.
3 F. M. Bautista, J. M. Campelo, A. Garcia, J. Leon, D. Luna and J. M. Marinas, *J. Chem. Soc., Perkin Trans. 2*, 1995, 815.
4 F. M. Bautista, J. M. Campelo, A. Garcia, R. Guardeño, D. Luna and J. M. Marinas, *J. Chem. Soc., Perkin Trans. 2*, 1989, 493.
5 J. M. Campelo, R. Chakraborty and J. M. Marinas, *Synth. Commun.*, 1996, **26**, 415.
6 J. M. Campelo, R. Chakraborty and J. M. Marinas, *Synth. Commun.*, 1996, **26**, 1639.
7 H. Hattori, *Chem. Rev.*, 1995, **95**, 537 and ref. therein.
8 D. Barthomeuf, *Catal. Rev. Sci. Eng.*, 1996, **38**, 521 and ref. therein.
9 Y. Ono and T. Baba, *Catal. Today*, 1997, **38**, 321 and ref. therein.
10 R. M. Martin-Aranda, M. A. Vicente-Rodriguez, J. M. Lopez-Pestaña, A. J. Lopez-Peinado, A. Jerez, J. D. Lopez-Gonzalez and M. A. Bañares-Muñoz, *J. Mol. Catal. A*, 1997, **124**, 115.
11 P. E. Hathaway and M.E. Davis, *J. Catal.*, 1989, **116**, 263.
12 P. E. Hathaway and M.E. Davis, *J. Catal.*, 1989, **116**, 279.
13 A. Auroux, P. Artizzu, I. Ferino, R. Monaci, E. Rombi and V. Solinas, *Microporous Mater.*, 1997, **11**, 117.
14 P. E. Hathaway and M.E. Davis, *J. Catal.*, 1989, **119**, 497.
15 N. K. Das and K. Pramanik, *J. Indian Chem. Soc.*, 1997, **74**, 701.
16 M. Lasperas, H. Cambon, D. Brunel, I. Rodriguez and P. Geneste, *Stud. Surf. Sci. Catal.*, 1995, **97**, 319.
17 J. C. Kim, H. X. Li, C. Y. Chen and M. E. Davis, *Microporous Mater.*, 1994, **2**, 413.
18 F. Yagi, H. Tsuji and H. Hattori, *Microporous Mater.*, 1997, **9**, 237.
19 F. Yagi and H. Hattori, *Microporous Mater.*, 1997, **9**, 247.
20 M. Huang and S. Kaliaguine, *Catal. Lett.*, 1993, **18**, 373.
21 K. R. Kloetstra and H. van Bekkum, *J. Chem. Soc., Chem. Commun.*, 1995, 1005.
22 K. R. Kloetstra and H. van Bekkum, *Stud. Surf. Sci. Catal.*, 1997, **105**, 43.
23 K. R. Kloetstra, J. van den Broek and H. van Bekkum, *Catal. Lett.*, 1997, **47**, 235.
24 K. R. Kloetstra, M. van Laren and H. van Bekkum, *J. Chem. Soc., Faraday Trans.*, 1997, **93**, 1211.
25 H. Lauron-Pernot, F. Luck and J. M. Popa, *Appl. Catal.*, 1991, **78**, 213.
26 C. Lahousse, J. Bachelier, J. C. Lavalley, H. Lauron-Pernot and A. M. Le Govic, *J. Mol. Catal.*, 1994, **87**, 329.
27 F. Audry, P. E. Hoggan, J. Saussey, J. C. Lavalley, H. Lauron-Pernot and A. M. Le Govic, *J. Catal.*, 1997, **168**, 471.
28 Savitsky-Golay, *Anal. Chem.*, 1964, **36**, 1627.
29 E. P. Barrett, L. S. Joyner and P. Halenda, *J. Am. Chem. Soc.*, 1951, **73**, 373.
30 G. Halsey, *J. Chem. Phys.*, 1948, **16**, 931.
31 J. M. Campelo, A. Garcia, D. Luna, J. M. Marinas and A. A. Romero, *Thermochim. Acta*, 1995, **261**, 175.
32 O. W. Florke, *Z. Kristallogr.*, 1967, **125**, 134.
33 F. d'Yboire, *Bull. Soc. Chim. Fr.*, 1962, 1762.
34 D. Muller, E. Jahn, G. Ladwig and U. Haubenreisser, *Chem. Phys. Lett.*, 1984, **109**, 332.
35 C. S. Blackwell and R. L. Paton, *J. Phys. Chem.*, 1984, **88**, 6135.
36 V. M. Mastikhin, I. L. Mudrakowsky, V. P. Shmachkova and N. S. Kotsarenko, *Chem. Phys. Lett.*, 1987, **139**, 93.
37 J. B. Peri, *Discuss. Faraday Soc.*, 1971, **52**, 55.
38 S. Brunauer, L. S. Deming, W. S. Deming and E. Teller, *J. Am. Chem. Soc.*, 1940, **62**, 1723.
39 K. S. W. Sing, D. H. Everett, R. A. W. Haul, L. Moscou, R. A. Pierotti, J. Rouquerol and T. Siemieniewska, *Pure Appl. Chem.*, 1985, **57**, 603.
40 W. D. Harkins and G. Jura, *J. Chem. Phys.*, 1943, **11**, 431.
41 J. C. P. Broekhoff and B. G. Linsen, in *Physical and Chemical Aspects of Adsorbents and Catalysts*, ed. B. G. Linsen, Academic Press, London, 1970, pp. 1–62.
42 A. Mata Arjona, J. B. Parra Soto and C. Otero Arean, *Stud. Surf. Sci. Catal.*, 1982, **10**, 175.
43 E. P. Parry, *J. Catal.*, 1963, **2**, 371.
44 M. R. Basila, T. B. Kantner and K. H. Rhee, *J. Phys. Chem.*, 1964, **68**, 3197.
45 M. R. Guisnet, *Acc. Chem. Res.*, 1990, **23**, 392.
46 C. Mercier, G. Allmang and M. Aufrand, *Appl. Catal. A*, 1994, **114**, 51.
47 D. Bassett and H.W. Habgood, *J. Phys. Chem.*, 1960, **64**, 769.

Paper 8/07538G